Full Length Article

Atomic structure and annealing-induced reordering of ε-Ga$_2$O$_3$: A Rutherford backscattering/channeling and spectroscopic ellipsometry study

Z. Zolnai [a],[*], P. Petrik [a],[b], A. Németh [c], J. Volk [a], M. Bosi [d], L. Seravalli [d], R. Fornari [d],[e]

[a] Centre for Energy Research, Institute of Technical Physics and Materials Science, P.O. Box 49, 1525 Budapest, Hungary
[b] Department of Electrical and Electronic Engineering, Institute of Physics, Faculty of Science and Technology, University of Debrecen, 4032 Debrecen, Hungary
[c] Wigner Research Centre for Physics, Institute for Particle and Nuclear Physics, Konkoly-Thege M. út 29-33, H-1121 Budapest, Hungary
[d] Institute of Materials for Electronics and Magnetism (IMEM-CNR), Viale delle Scienze 37/A, 43124 Parma, Italy
[e] Dept. of Mathematical, Physical and Computer Sciences, University of Parma, Viale delle Scienze 7/A, 43124 Parma, Italy

A B S T R A C T

The crystallographic structure of thin Ga$_2$O$_3$ layers grown by metal–organic vapour phase epitaxy on Al$_2$O$_3$ substrate was analyzed by Rutherford Backscattering Spectrometry/Channeling (RBS/C) angular yield scans performed around the c-axis of as-grown Ga$_2$O$_3$. The measured widths and minimum yields of the scan curves for the Ga and O component were compared to calculations based on the continuum steering potential model. The results obtained are consistent with a crystal structure containing oxygen atoms arranged in a 4H hexagonal closely packed lattice and Ga atoms preferentially occupying octahedral interstitial sites in the 4H cells - a structure closely related to the ε-Ga$_2$O$_3$ polymorph. After high-temperature annealing remarkable structural transformation is detected via significant changes in the RBS/C spectra. This effect is related to the hexagonal-monoclinic, i.e., ε-β phase transformation of Ga$_2$O$_3$. Spectroscopic ellipsometry spectra of as-grown and annealed samples can be best fitted using a vertically graded single-layer B-spline model. Significant differences in the dielectric functions were found, showing bandgap reduction for long term annealing. These features are related to the ε-β polymorphic transformation, variation of the preferred crystallographic orientation upon annealing, and differences in residual strain and defect structure determined by the annealing conditions.

1. Introduction

Due to its extra-wide bandgap (E$_g$ > 4.5 eV) gallium oxide (Ga$_2$O$_3$) has become a favoured candidate for a number of applications [1], such as solar-blind detectors for the UV-C radiation range (wavelengths below 280 nm) and power electronics because of its high critical breakdown field, estimated to be higher than that of SiC and GaN [1].

Most scientific research has so far focused on monoclinic β-Ga$_2$O$_3$, as it is the thermodynamically stable polymorph. However, β-Ga$_2$O$_3$ exhibits anisotropic physical properties, and the single crystals are prone to cleavage thus leading to practical problems in device manufacturing. Accordingly, there is an increasing interest about other Ga$_2$O$_3$ polymorphs, the less explored α, γ, δ, and ε phases [2–4] as they generally possess a crystallographic structure with higher symmetry and lower anisotropy than the monoclinic β-phase. However, they are metastable and tend to convert to β-phase at elevated temperatures or at low growth rates (i.e., very low supersaturations) [5–8]. It is thus important to identify and describe different polymorphs as well as to follow temperature-induced phase transitions in Ga$_2$O$_3$ substrates and epilayers. The role of suitable experimental characterization techniques becomes increasingly important for such purposes.

Besides X-ray diffraction [2,9], neutron diffraction [4], and transmission electron microscopy (TEM) [2,8,10], Rutherford Backscattering Spectrometry (RBS) in combination with channeling (RBS/C) have been applied for the analysis of atomic composition and crystalline quality as well as for the quantitative characterisation of the crystal structure of different semiconductors. By means of RBS/C, valuable structural information can be extracted for elementary and multi-component materials as a function of depth for epitaxial layers and substrates as well as for their interfacial matching properties accompanying epitaxial layer growth. In addition, RBS/C can provide information about the localization of dopant atoms in crystalline materials. In this case, impurities occupying interstitial or substitutional lattice sites can be distinguished, e.g., localization analysis of Er dopants in Ga$_2$O$_3$ can be successfully performed and post implantation annealing-induced recrystallization of the Ga$_2$O$_3$ matrix can be observed [11–14]. In general, implantation-induced disorder formation in binary semiconductors can be followed separately in the different sublattices by RBS/C with optimal choice of

the probing ion beam and analyzing ion energy [15]. Moreover, multi-axial channeling experiments performed along different crystallographic axes yield information on preferential ordering of implantation-induced lattice disorder due to the presence of uniaxial lattice strain [16]. As it was recently shown, interplay effects between disorder and strain in Ga_2O_3 provides an additional degree of freedom to modify the rate of the polymorphic transitions from the β-phase to other Ga_2O_3 polymorphs [17]. To date, RBS/C analysis has been applied mainly to describe implantation induced disorder and its recovery after high temperature annealing [11–14] in β-Ga_2O_3 and less attention has been paid to detailed RBS/C angular scan measurements, which provides information on the critical angles of channeling in the Ga and O sublattices in different polymorphs of Ga_2O_3.

The so-called ε-phase of Ga_2O_3 was first observed in β-contaminated precipitates [2], later neutron diffraction studies showed that it belongs to a hexagonal system with space group $P6_3mc$ [4], with a ratio of octahedral/tetrahedral gallium atoms of 2.2:1 located between close-packed oxygen layers. A detailed investigation of the real crystal structure of ε-Ga_2O_3 revealed that the arrangement of Ga-hosting tetrahedra and octahedra is not random, and that ordering occurs at the nanoscopic scale [9,10]. The structure is made of a 4H hexagonal close-packed (HCP) oxygen sublattice with stacking sequence ABAC along the c-axis, while the Ga atoms occupy octahedral and tetrahedral sites forming two types of polyhedral layers parallel to the c-plane. The real microscopic structure is indeed orthorhombic with $Pna2_1$ space group symmetry, analogous to that of κ-Al_2O_3. Indeed, ε-Ga_2O_3 shows up as hexagonal (ε) or orthorhombic (κ), depending on the size of the ordered domains and resolution of the applied characterization probe. Actually, due to the very small size of the orthorhombic domains, they were clearly detectable only by electron diffraction experiments with high lateral resolution. This fact is at the basis of the ambiguity in the current literature nomenclature, which indifferently uses ε or κ for the same Ga_2O_3 polymorph. For epitaxy and device technology purposes ε-Ga_2O_3 can be regarded as a pseudo-hexagonal semiconductor, with the space group similar to that of GaN and AlN, which makes this material especially useful in the development of novel devices based on nitride/oxide structures.

In the following, we shall maintain the name ε but the reader must remember that the studied material is not genuinely hexagonal, but rather constituted of orthorhombic 120° rotational domains. This is justified as the applied experimental methods provide results averaged over numerous domains and highlight the long-range hexagonal symmetry.

We performed detailed angular scan measurements with 2-MeV He^+ RBS/C on as-grown ε-Ga_2O_3 thin layers epitaxially grown on α-Al_2O_3 substrates. The width of the angular scan curves and the minimum backscattering yields were determined separately for the Ga and O sublattices. The obtained values were compared to those estimated from calculations based on the structure of an HCP oxygen lattice with Ga atoms distributed at tetrahedral and octahedral lattice sites between the oxygen sheets – i.e. the structure identified for ε-Ga_2O_3 [4,10]. Besides valuable information gained on as-grown ε-Ga_2O_3 and its annealing-induced phase transition, our RBS/C experiments may pave the way toward the lattice localization analysis of e.g. Er [11] or Sn [18] dopants to quantify the degree of substitutional lattice site occupation and electrical activation of dopants in Ga_2O_3 crystals.

Spectroscopic ellipsometry (SE) has been frequently applied in the characterization of different Ga_2O_3 polymorphs. However, the investigated samples were prepared under different experimental conditions and the measured SE data have been evaluated based on various model assumptions [19–23]. In general, refractive indices and bandgaps reported for monoclinic and hexagonal Ga_2O_3 differ moderately and the ranges of the reported values for distinct polymorphs may overlap. E.g., for hexagonal and monoclinic phase Ga_2O_3 the reported bandgaps fall within 4.5–5 eV and 4.5–4.9 eV, while refractive indices were found to have values between 1.74 and 1.95 and 1.68–1.89, respectively [1,24].

To further elucidate possible peculiarities of the polymorphs a practical approach follows the change of the optical properties upon phase transition of the material for samples with well explored crystalline structure and nanoscale ordering properties.

In this work, the optical properties of Ga_2O_3 layers – such as dielectric function, absorption edge - were determined from SE measurements before and after annealing. The crystalline ordering and nanoscopic structure of the samples have been previously described in detail by TEM and XRD analysis [5,9,10]. Also, additional information was extracted from RBS/C experiments as complementary characterization technique reported in this paper. The annealing induced optical property changes revealed by SE, and their possible relation to phase transformation and structural changes will be discussed.

Our approach, combining RBS/C and SE, provides the opportunity to shed light on the correlation between crystal symmetry, crystalline quality, interfacial, structural, and optical properties of as-grown and annealed ε-Ga_2O_3 layers, as a function of depth on the nanoscale.

2. Experimental

The epitaxial growth of thin Ga_2O_3 layers was performed using a MOVPE (metal–organic vapour phase epitaxy) stainless steel reactor. The epilayers were deposited on (0001) α-Al_2O_3 substrates at a temperature of 650 °C using trimethylgallium (TMG) and ultrapure water as precursors, while ultrapure H_2 was used as carrier gas. The thickness of the thin film varied in the range of 250–350 nm. For annealing experiments, a set of specimens with the size of about 6×6 mm^2 were cut from the Al_2O_3 substrates with deposited epilayers on top. The selected samples were cleaned with organic solvents and then placed within a tubular furnace with controlled inner atmosphere. The annealing was performed at 1000 °C in oxygen atmosphere in order to prevent layer decomposition. The annealing time was 2 h with cooling rate of 2 °C/min, or 6 h with higher cooling rate of 7.5 °C/min [5] at the end of the heat treatment, in order to see the effect of the annealing parameters on the structural changes. Complete phase conversion from ε-Ga_2O_3 to the β-Ga_2O_3 phase occurred for both annealing times. More details on the growth and annealing processes are reported in Ref. [5].

The 2-MeV He^+ RBS/C experiments were performed in a sample chamber connected to the 5-MV Van de Graaff accelerator operated at the Wigner Research Centre for Physics, Institute for Particle and Nuclear Physics in Budapest. In the scattering chamber the vacuum was $\sim 10^{-4}$ Pa. To reduce the hydrocarbon deposition, liquid N_2 cooled traps were used along the beam path and around the wall of the chamber. The channeling experiments were carried out using a two-axis goniometer system capable of determining the target orientation with a precision of 0.01° both in tilt and azimuthal dimensions. In the 2-MeV $^4He^+$ RBS/C measurements, the He^+ beam was collimated to dimensions of 0.4×0.4 mm^2, while the beam divergence was kept below 0.05°. Low beam current of ~ 10 nA was used to reduce the damage created by the analyzing beam itself [25]. The beam current was measured by a transmission Faraday cup [26]. Backscattered He^+ ions were detected using an ORTEC surface barrier detector mounted in Cornell geometry at a the scattering angle of 165°. The energy resolution of the detection system was 15 keV. The measurement of the aligned spectra of as-grown Ga_2O_3 was carried out using a He^+ ion beam oriented precisely parallel to the ⟨0001⟩ axis of Ga_2O_3 after a refined tilt angle scan procedure with the minimalization of the backscattering yield from the near surface region of the sample. Random spectra were recorded while the sample was continuously rotating around the sample normal tilted off by 15° from the analyzing ion beam to avoid both axial and planar channeling of the helium projectiles. To avoid ion beam-induced charging [27] and the build-up of a surface electric potential on the poorly conducting Ga_2O_3/Al_2O_3 samples, an electron flood gun source was applied during the RBS/C measurements. Experimental RBS spectra were evaluated by the RBX code [28].

The layer thicknesses and the dielectric functions were measured by

a Woollam M-2000DI spectroscopic ellipsometer at the angles of incidence of 55°, 65° and 75°. Spectra of $\Psi = \tan^{-1}(|r_p/r_s|)$ and $\Delta = \arg(r_p/r_s)$ were measured, where r_p and r_s are the complex reflection coefficients of light polarized parallel and perpendicular to the plane of incidence, respectively. The structure of the sample was described by an optical model that consists of an Al_2O_3 substrate and a graded layer, in which the dielectric function of the materials is described by B-splines with a node distance of 0.4 eV.

The results of previous TEM analysis [10], performed on a thinned specimen prepared from the as-grown sample were used in the interpretation of the RBS/C and SE measurements. Crystal cell parameters derived from XRD [9] and TEM [10] were taken into account for calculation of RBS/C angular yield scan parameters - critical angle for channeling, minimum yield - for the different model structures of the Ga_2O_3 layer and for the Al_2O_3 substrate. Also, micro- and nanostructural information provided by TEM and XRD was considered in the evaluation of in-depth structural and optical property changes observed by RBS/C and SE before and after annealing.

3. Results and discussion

3.1. RBS/C measurements on as-grown Ga_2O_3

RBS analysis in combination with channeling was performed on the as-grown Ga_2O_3 layer. First the sample was tilted to 7° and rotated in the azimuth angle range of 0°-360°, thus following the common procedure to find dips in the backscattering yield at certain azimuth angles [29] the minima of which corresponds to the planar channeling directions of the analyzing He$^+$ ions along the equivalent crystallographic planes of the crystal. Nevertheless, in our sample we were unable to find such planar minima as only slight fluctuations have been detected in the RBS yield upon rotation of the sample. On the other hand, clear axial channeling effect was revealed in the vicinity of zero tilt angle, and it was possible to refine the axial channeling direction by varying the sample tilt angle in small steps. These findings are consistent with the 10–20 nm crystallographic domains, rotated in-plane with respect to each other, already observed by TEM. Such arrangement appears as a columnar structure with column axis perpendicular to the Ga_2O_3 sample surface [10]. The lack of in-plane long-range order on the lateral scale, as detected also by RBS/C, is due to the macroscopic ion beam size, being several orders of magnitude larger than the domain size of crystallites in the Ga_2O_3 layer. On the other hand, the nanoscopic crystallographic domains are highly oriented along the axis nearly perpendicular to the sample surface, i.e., the c-axis, as it can be concluded from the strong axial channeling effect and small minimum yield for Ga (see Figs. 1 and 2).

Fig. 1(a) shows the random and best oriented RBS/C spectra of the as-grown sample. The spectral edges for the elements of Ga, O, and Al,
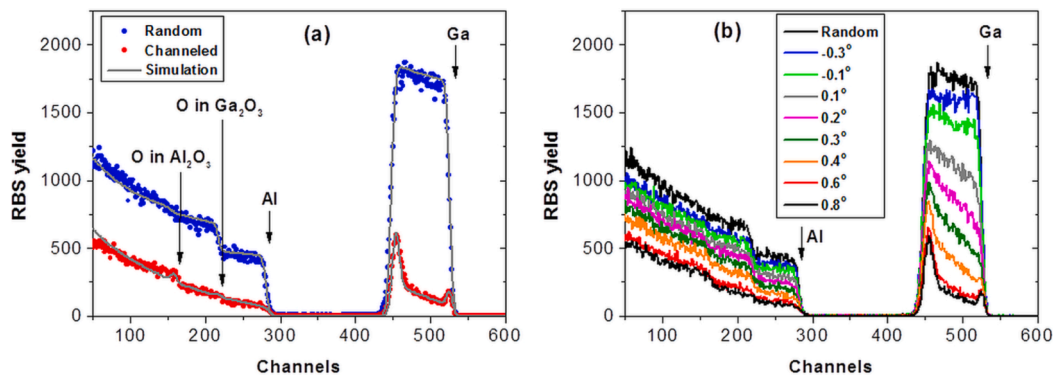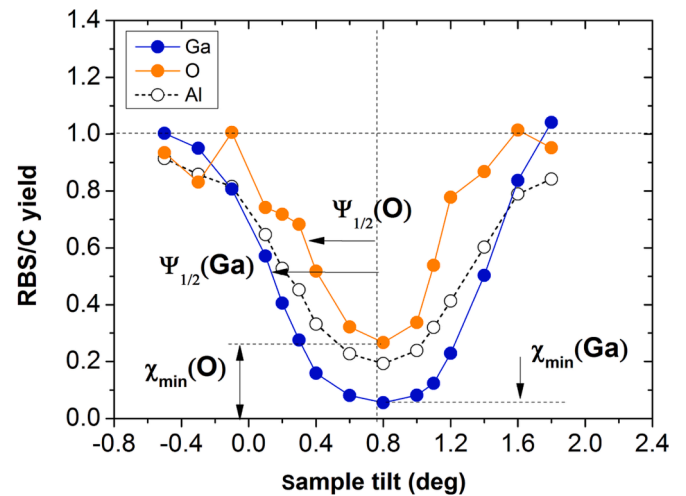
Fig. 2. 2 MeV He$^+$ RBS/C angular scan curve for the Ga and O components measured around the ⟨0001⟩ axis of ε-Ga_2O_3. Critical angles for channeling ($\Psi_{1/2}$) and minimum yields (χ_{min}) are indicated. Angular yield data for Al in the underlying α-Al_2O_3 substrate are also shown for comparison.

originating either from the Ga_2O_3 layer or from the buried sapphire substrate, are indicated. For Ga, a sharp surface peak can be observed in the channeling spectrum (channel no. ∼ 525), and the minimum yield (channel no. ∼ 510) is about 5 %, being close to the value of a good quality single crystal. Our minimum yield is better than the value of ∼ 10 % presented for ⟨-201⟩ β-Ga_2O_3 in Ref. [11] and it is comparable to that observed for β-Ga_2O_3 prior to ion implantation in another work [12]. Besides the Ga component we can also estimate the oxygen yield right below the surface of Ga_2O_3 (channel no. ∼ 200 for O) if the Al signal background originating from the sapphire substrate is appropriately subtracted. This way the Ga and O sublattices of Ga_2O_3 can be separately analysed in the RBS/C spectra.

Solid lines in Fig. 1(a) show RBX [28] simulations for the random and channeled spectrum. For the oriented case, three parameters were used in RBX to reconstruct the measured data: the surface peak intensity, the minimum yield right below the surface peak and the gradient of the dechanneling background. These three parameters were independently optimized for the two components of the Ga_2O_3 layer and of the Al_2O_3 substrate. As a note, in a previous work on ion implanted silicon carbide, RBS channeling spectra were successfully reconstructed by RBX simulations during the evaluation of disorder depth profiles in both the Si and C sublattices of 6H-SiC [15].

From the RBS spectra, element specific depth scales for each component of the different layers in the sample can be defined through

Fig. 1. (a) Random and channeling 2 MeV He$^+$ RBS/C spectra of the ⟨0001⟩-oriented ε-Ga_2O_3 layer epitaxially grown on an Al_2O_3 substrate. Spectrum edges for different elements in the thin layer and in the underlying substrate are indicated. Solid lines show RBX simulations. (b) Measured RBS spectra of the same layer structure as a function of tilt angle with respect to the sample normal.

an energy-to-depth conversion process. This procedure, for each element, gives zero depth (surface) positions on the energy scale (see the arrows in Fig. 1(a)) and in-depth scales along the energy scale, based on knowledge of the measurement geometry, the element specific kinematic K-factors and ion stopping powers as well as real atomic densities in the different layers: for the present experimental case either the Ga_2O_3 layer or the underlying Al_2O_3 substrate. More details on energy-to-depth conversion can be found, e.g. in Refs. [15] and [28].

At channel no. 455 in Fig. 1(a) there is a sharp increase in the Ga yield (red dots) indicating the presence of point defects, extended defects, and/or strain at the Ga_2O_3/Al_2O_3 interface. Furthermore, the presence of a different crystal lattice structure with slightly modified crystallographic orientation compared to the topmost Ga_2O_3 layer may also be responsible for the increased RBS yield. Detailed TEM analysis [10] revealed the presence of a thin γ-Ga_2O_3 intermediate layer at the Ga_2O_3/Al_2O_3 interface, which could well explain the results of RBS/C analysis. Actually, the RBX simulation under channeling conditions shows the presence of a thin intermediate layer at the interface, whose dechanneling contribution is nearly equivalent to that of a fully disordered layer with effective thickness of about 15 nm (see the solid line at channel no. 455 in Fig. 1(a)). This result is consistent with TEM observations [10] revealing that the intermediate layer thickness varies in the range of 10–50 nm. Recently, the presence of an intermediate layer was confirmed also by other research groups [30,31].

Fig. 1(b) shows RBS/C spectra for the as-grown Ga_2O_3 layer on Al_2O_3 substrate as a function of tilt angle with respect to the sample surface. As the tilt angle varies in steps of 0.1° from random toward channeling direction, significant yield drops can be observed in the whole spectrum energy range.

Fig. 2 shows RBS/C angular scans, i.e., RBS yield vs. tilt angle with respect to the sample normal of the as-grown Ga_2O_3 layer, separately for the Ga and O sublattices. Significant differences appear both for the half width at half maximum (HWHM), that is, the critical angle for axial channeling, $\Psi_{1/2}$, and for the minimum yield, χ_{min}, of the Ga and O angular scan curves. Here χ_{min} is the minimum of the angular yield normalized to the random yield, measured right under the surface of the crystal. For Ga and O, values of $\Psi_{1/2} = 0.63°$ ($\pm 0.02°$) and $\Psi_{1/2} = 0.38°$ ($\pm 0.03°$) can be revealed. The corresponding minimum yields are $\chi_{min} \sim 0.05$ and $\chi_{min} \sim 0.24$, for Ga and O, respectively. In Fig. 2, the position of the minima, i.e., χ_{min} in the angular scans appears at a sample tilt angle of $\sim 0.78°$, revealing that this angular position corresponds to the $\langle 0001 \rangle$ axial channel direction of the ε-Ga_2O_3 layer.

In order to relate the measured $\Psi_{1/2}$ values to the crystal structure of the Ga_2O_3 epilayer, we compared them to those estimated from a semiempirical continuum steering potential model for axial channeling [32] which is based on the following expression [16]:

$$\Psi_{1/2} \text{ (deg)} = 0.8 \times F_{RS}(\xi) \times \Psi_1 \tag{1}$$

where

$$\Psi_1 \text{ (deg)} = 0.0971 \times [Z_1 \langle Z_2 \rangle / (E_0 \langle d \rangle)]^{1/2} \tag{2}$$

Here Ψ_1 is the Lindhard critical angle for channeling, $F_{RS}(\xi)$ is the square-root of the Moliére string potential, where $\xi = m\langle u \rangle / a_{TF}$, and $\langle u \rangle$ and a_{TF} are the root-mean-square (r.m.s.) thermal displacement and the Thomas-Fermi screening radius, respectively, while $m = 1.2$ is an universal fitting parameter [16,32]. Z_1 and $\langle Z_2 \rangle$ denote the atomic number of the projectile and the average atomic number of the host atoms on the axis of channeling, E_0 (MeV) is the incident ion energy and $\langle d \rangle$ (nm) is the mean interatomic spacing along the axial channel direction. According to the charge-state equilibrium of energetic ions passing through solid targets [33], the 2-MeV He projectiles are expected to be fully ionized with charge state of $+2$. For fully ionized projectiles the Thomas-Fermi screening radius is $a_{TF} = 0.885a_0 / \langle Z_2 \rangle^{1/3}$ [32], where a_0 is the Bohr radius. In general, Eq. (1) gives the critical angle for axial channeling with sufficient accuracy for a wide range of target materials

[32].

Previous experiments [4] have shown that the structure of ε-Ga_2O_3 consists of gallium atoms distributed over three partially occupied sites, with an octahedral/tetrahedral (O_h/T_d) ratio of 2.2:1, embedded in a close-packed hexagonal oxygen lattice of 4H-type. The cell parameters were found to be c = 9.255 Å and a = 2.906 Å [9], respectively. Fig. 3(a) shows schematics of the ABAC stacking sequence of the 4H hexagonal oxygen lattice together with O_h and T_d interstitial site locations. Octahedral sites in the 4H cell form sheets with a stacking sequence of *ccbb*. These sheets are located in between the oxygen layers which follow the ABAC sequence. Tetrahedral sites in the body of the 4H cell form sheets with stacking sequence *bbcc* in between the oxygen layers. In addition, T_d sites are also located along the six edges and along the centerline of the hexagonal cell, connecting oxygen atoms in adjacent A-sheets along the $\langle 0001 \rangle$ axis. Considering that the atoms located on cell surfaces and in cell apices are shared by adjacent cells, the 4H cell contains twelve oxygen atoms, twelve O_h sites and twenty-four T_d sites.

According to the Ga:O stoichiometry, in ε-Ga_2O_3 the Ga atoms occupy only a fraction of the interstitial sites. Considering such crystal structure one may estimate the composition of the atomic strings along the c-axis, i.e. the $\langle 0001 \rangle$ axial channel of ε-Ga_2O_3. As it can be deduced, different mixed atomic strings containing both Ga and O atoms appear with $\langle Z_2 \rangle$ and $\langle d \rangle$ determined by the Ga occupancy of the O_h and T_d sites.

Supposing that all Ga atoms occupy O_h sites and otherwise they are randomly distributed so that the average occupancy of O_h sites is 2/3, then the Ga atoms together with the O atoms in the B- and C- sheets (see Fig. 3(a)) form mixed Ga-O atomic rows with effective parameters $\langle Z_2 \rangle = 21$ and $\langle d \rangle = 0.397$ nm for the formation of continuum steering potential. However, in this case oxygen atoms in the A-sheets (see Fig. 3(a)) form pure O-O strings with $\langle Z_2 \rangle = 6$ and $\langle d \rangle = c/2 = 0.463$ nm along the $\langle 0001 \rangle$ axis. One may notice a large $\langle Z_2 \rangle$-contrast and a difference also in the average interatomic spacings between the two types of atomic rows. Such conditions can result in significantly different critical angles for channeling.

On the other hand, when all Ga atoms are supposed to be located in T_d sites and are otherwise randomly distributed, giving an average T_d site occupancy of 1/3, then two types of mixed Ga-O atomic rows can be formed along the $\langle 0001 \rangle$ axis: one connecting the oxygen sheets A (hereinafter called A-rows), and - from the sense of RBS channeling - two identical ones which connect oxygen sheets B or C (hereinafter called B-, and C-rows). For the A-rows $\langle Z_2 \rangle = 17.3$ and $\langle d \rangle = 0.278$ nm while for the B- and C-rows $\langle Z_2 \rangle = 17.3$ and $\langle d \rangle = 0.556$ nm can be ascertained for the mixed Ga-O atomic strings. Note, for this kind of Ga atomic configuration, the two different types of atomic strings can be described with similar $\langle Z_2 \rangle$ values but largely different interatomic spacings. Such relations are also expected to result in distinct critical angles for $\langle 0001 \rangle$ axial channeling.

Using the actual $\langle Z_2 \rangle$ and $\langle d \rangle$ values, and considering $\langle u^2 \rangle_{Ga} = 0.0044$ Å^2 and $\langle u^2 \rangle_O = 0.0091$ Å^2 for the thermal displacement of Ga and O atoms [4], the critical angles for channeling along the c-axis can be calculated according to Eq. (1) and Eq. (2), for both mixed Ga-O and monoatomic O-O strings, for the schematic crystal structures described above. The results of these calculations are summarized in Table 1. Uncertainties ($\Delta\Psi_{1/2}$, when considered) for the calculated $\Psi_{1/2}$ values are related to different r.m.s. thermal vibrational amplitudes for the Ga and O atoms thus giving rise to uncertainty in the Moliére string potential.

As expected, the calculated critical angles show striking differences between the two types of atomic strings (A-rows and B-/C-rows) both for pure O_h and pure T_d site occupation by Ga atoms. Nevertheless, an apparently better agreement can be found between calculated and experimental $\Psi_{1/2}$ values for pure O_h interstitial site localization of Ga. Indeed, refined structure analysis has shown much higher O_h site occupancy by Ga for the ε-Ga_2O_3 polymorph [4]. The structure associated with such an asymmetric O_h/T_d site configuration is rather close to that of α-Ga_2O_3 in which the Ga atoms all occupy O_h sites [4], and to that of α-Al_2O_3 corundum [34,35].
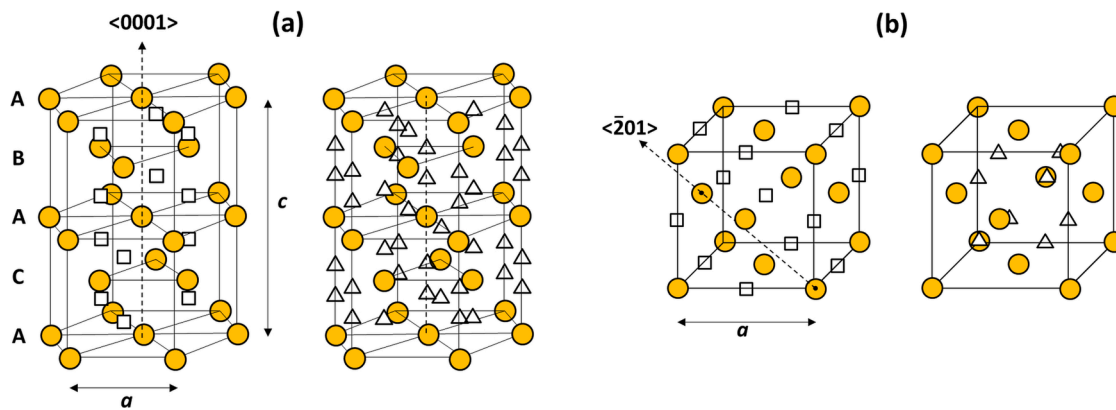
Fig. 3. Schematic crystal structure of (a) a 4H hexagonal closely packed (HCP) oxygen lattice and (b) a face centered cubic (FCC) oxygen lattice, which are closely related to the structure of the (a) ε-Ga$_2$O$_3$ and (b) β-Ga$_2$O$_3$ polymorphs, respectively [4]. Oxygen atoms are marked by yellow dots while Ga atoms occupy octahedral (O$_h$) and tetrahedral (T$_d$) interstitial sites (marked by open squares and triangles) in the oxygen sublattice with probabilities according to the Ga$_2$O$_3$ stoichiometry. The ⟨0001⟩ direction, i.e., c-axis for (a) and the ⟨-201⟩ axis for (b) are represented by arrows. For more details see the text. (For interpretation of the references to colour in this figure legend, the reader is referred to the web version of this article.)

Table 1
Calculated critical angles for channeling ($\Psi_{1/2}$) with their uncertainties ($\Delta\Psi_{1/2}$) for 2-MeV He$^+$ ions and for different polymorphs of Ga$_2$O$_3$ with various Ga occupancies of octahedral (O$_h$) and tetrahedral (T$_d$) sites. Different types of atomic rows viewed along the axis of channeling are marked as A, B, and C-rows. Average interatomic spacings, (⟨d⟩) and the type of composition of the atomic rows, mixed or monoatomic, are indicated. The panel with missing polymorph identification accounts for a tentative structure where all Ga atoms occupy tetrahedral interstitial sites in the 4H oxygen lattice. Experimental $\Psi_{1/2}$ values measured separately for the Ga and O component are also given for comparison.

Polymorph	Oxygen lattice	Axis	Atomic row	Row type	O$_h$ site Ga occupancy	T$_d$ site Ga occupancy	⟨d⟩ (Å)	$\Psi_{1/2}$ (deg.)	$\Delta\Psi_{1/2}$ (deg.)
ε	4H	⟨0001⟩	A	mixed	–	10%	3.85	0.46	±0.02
			B/C	mixed	45 %	10%	4.4	0.54	±0.03
α	4H	⟨0001⟩	A	monoatomic (O)	–	0%	4.63	0.34	
			B/C	mixed	67 %	0%	3.97	0.59	±0.03
–	4H	⟨0001⟩	A	mixed	–	33%	2.78	0.73	±0.04
			B/C	mixed	0%	33%	5.56	0.51	±0.03
β	FCC	⟨−201⟩	A	monoatomic (O)	–	–	5.14	0.33	
			B	monoatomic (Ga)	33%	–	15.4	0.36	
			C	monoatomic (Ga)	–	16%	30.8	0.26	
Experimental values									
O component								0.38	±0.03
Ga component								0.63	±0.02

For comparison, the $\Psi_{1/2}$ values calculated for a O$_h$/T$_d$ site occupation of 2.2:1 for Ga are also represented in Table 1. This structure has been identified as the ε-phase [4,10]. Note that in this case for A-rows ⟨Z$_2$⟩ = 12.2 and ⟨d⟩ = 0.385 nm while for B/C-rows ⟨Z$_2$⟩ = 20 and ⟨d⟩ = 0.44 nm can be considered. For this atomic configuration the agreement of $\Psi_{1/2}$ with experimental values is somewhat weaker than for pure O$_h$ site occupancy but is still much better when compared to the case of pure T$_d$ site localization of Ga (see the tentative structure with lacking polymorph identification in Table 1).

From the above considerations it can be concluded that for Ga atoms the angular yield for dechanneled He projectiles travelling through the c-axis may be governed by the B- and C-rows in the 4H lattice of ε-Ga$_2$O$_3$. These atomic rows altogether contain more Ga atoms and possess higher $\Psi_{1/2}$ critical angles compared to the A-rows, according to the semi-empirical model calculations above. On the other hand, for oxygen atoms, the angular yield given by the dechanneled He fraction can be controlled by the A-rows which can be described by a lower average atomic number and a smaller $\Psi_{1/2}$ value in the 4H oxygen lattice structure when compared to the B- and C-rows.

Note that, from a structural point of view, certain features of the investigated Ga$_2$O$_3$ layer may affect our experimental results. TEM analysis revealed the presence of defects in the as-grown crystalline thin layer, i.e., twin boundaries and anti-phase boundaries were readily identified [10]. Such imperfections introduce local structural deviations which can cause perturbation to the channeling effect to certain degree.

It is also worth noting that, in agreement with its non-centrosymmetric *Pna2$_1$* space group, the positive and negative charges barycenters in ε-Ga$_2$O$_3$ do not coincide, giving rise to uncompensated electrical dipoles. This feature is also reflected by the out of plane distances of ∼ 0.1 Å (comparable with thermal displacements) of the Ga atoms with respect to the mean oxygen layers, adjacent along the c-axis, as determined by TEM [10]. The presence of such cationic displacements confirms the recently unveiled ferroelectric nature of the compound [9]. Nevertheless, the ⟨0001⟩ RBS/C angular yields are expected to be scarcely affected by the small out-of-plane cationic displacements along the c-axis, instead angular scans performed with low energy ions along another main crystallographic axes which are tilted off from the ⟨0001⟩ direction may be noticeably influenced. This is because $\Psi_{1/2}$ is closely associated with the mean lattice displacement distance measured perpendicular to the corresponding axis, and so its value reflects the degree of lattice distortions in the corresponding crystallographic plane [16]. Note that, in our case axial channeling by RBS can only be achieved along the c-axis, due to lack of long-range order in the c-plane of the ε-Ga$_2$O$_3$ epilayer, as mentioned above.

The presence of A-, B-, and C-atomic rows in ⟨0001⟩ ε-Ga$_2$O$_3$ lead to a different situation as compared to, for example, wurtzite ZnO or 6H-SiC viewed along the c-axis. In those semiconductors Zn-O and Si-C mixed atomic rows are formed, but only one type of atomic strings can be identified due to the higher symmetry of the crystal structure. Along the mixed atomic rows of ⟨0001⟩-oriented ZnO (6H-SiC) the channeled ions

experience an average steering potential created by the alternating Zn and O (Si and C) atoms on the axis, thus resulting in the same angular width $\Psi_{1/2}$ for the Zn and O (Si and C) sublattices. Since in these materials all the mixed atomic rows are similar, the angular yield curve for the two sublattices will overlap. E.g., 3.035 MeV He^+ channeling for $\langle 0001 \rangle$-oriented ZnO thin layers results in an angular width of $\Psi_{1/2} \sim 0.5°$ for both the Zn and O sublattices [36], while 0.94 MeV D^+ channeling for $\langle 0001 \rangle$-oriented 6H-SiC shows a $\Psi_{1/2}$ value of ~0.6° for both the Si and C components [16], respectively. These values agree within ±0.02° with calculations based on Eq. (1) and Eq. (2) using appropriate r.m.s. thermal displacement values for ZnO [37] and SiC [38], thus showing the applicability of the continuum steering potential model for axial channeling in multi-component solids. Note, also good agreement between experimental and calculated $\Psi_{1/2}$ values was found for 500 keV N^+ ions [15] impinging $\langle 0001 \rangle$-oriented 6H-SiC.

On the other hand, axial channeling along the c-axis of ε-Ga_2O_3 seems to be rather similar to the case of axial channeling along the $\langle 1$-$102 \rangle$ or $\langle 10$-$11 \rangle$ axis of 6H-SiC, where two different types of monoatomic rows comprising only Si or C atoms are formed with relatively high $\langle Z_2 \rangle$ contrast which results in ca. 34% lower $\Psi_{1/2}$ value for the C sublattice compared to the Si one [16].

For comparison, Table 1. also contains information on different atomic rows formed along the $\langle -201 \rangle$ axial channel of the β-Ga_2O_3 polymorph. However, the structure of the β-phase will be discussed later.

Besides the critical angle for channeling, another key parameter describing the angular scan curve is the minimum yield, χ_{min}. As Fig. 2 shows, significantly higher minimum yield can be observed for the angular scan curve of oxygen compared to that of gallium. This fact can be understood considering the high $\langle Z_2 \rangle$ contrast between the A-rows and B/C-rows, and, accordingly, the lower $\Psi_{1/2}$ value for the A-rows which contain mainly oxygen atoms. As it was shown, when channeled projectiles are steered between different atomic strings, the minimum yield of the string of the weaker steering potential, besides its own contribution, has also an additional component originating from the impact of the adjacent atomic strings of the stronger steering potential. This cross effect has been demonstrated e.g. for monoatomic Nb- and C-rows in $\langle 110 \rangle$ aligned NbC [39] and for monoatomic Si- and C-rows in $\langle 100 \rangle$-aligned 3C-SiC [40] single crystals (Note, here C-row means an atomic string containing carbon atoms only). In these works, the relatively large χ_{min} values for the C-rows were attributed to strong contributions from the Nb-rows (NbC) and Si-rows (SiC) steering the channeled projectiles with their deflection angles $\Psi_{1/2}$ into the C-rows. A similar effect can be anticipated in $\langle 0001 \rangle$-oriented ε-Ga_2O_3 for the A-rows and B/C-rows, resulting in a relatively high χ_{min} value for the former one, i.e., for oxygen atoms. The minimum yield for A-rows can be calculated as [39]:

$$\chi_{min}^A = 18.8[(N\langle d \rangle \langle u^2 \rangle)_A + K(N\langle d \rangle \langle u^2 \rangle)_{B,C}], \qquad (3)$$

where N is the atomic density of Ga_2O_3 estimated from its mass density of 6.06 g cm^{-3} [4], and the factor K is proportional to the relative scattering power from the different rows and can be estimated from the continuum string potential parameters to be $K = \langle Z_2 \rangle_{B,C} \langle d \rangle_A / (\langle Z_2 \rangle_A \langle d \rangle_{B,C})$. The second term in Eq. (3) gives the contribution from the B/C-rows to the χ_{min} of A-rows. This contribution seems to be significant, as the second term gives a χ_{min} value of 0.127, while the first term results in 0.077, respectively. Therefore, for A-rows a total minimum yield of χ_{min} = 0.204 can be estimated. On the other hand, for the B/C-rows a χ_{min} value of 0.035 can be calculated. Therefore, there is a satisfactory agreement between the calculations and the measured values of χ_{min} (Ga) = 0.05 and χ_{min} (O) = 0.24, when the cross-steering effect is taken into account. In conclusion, similarly to the $\Psi_{1/2}$ values, the minimum yield trends are quite consistent with the Ga_2O_3 model structure where Ga atoms predominantly located in the octahedral interstitial sites of the 4H oxygen sublattice.

Fig. 2 also shows He^+ angular yield data for the Al component of the underlying (0001) α-Al_2O_3 substrate for comparison. The background free RBS spectrum of the Al sublattice of sapphire (see the spectral range between channels no. 230–290 in Fig. 1(a)) enables the evaluation of the Al angular scan curve with a good accuracy. The angular scan for Al shows the appearance of the minimum yield, χ_{min}, at the tilt angle of about 0.78°, i.e., at similar position as that for χ_{min} of Ga and O. Also, all the three curves show similar symmetries around the tilt angle of 0.78°. This reveals a good matching between the c-axis directions of the Ga_2O_3 layer and the underlying Al_2O_3 substrate, confirming the high quality of the epitaxial growth.

In Fig. 2 a critical angle of $\Psi_{1/2} \approx 0.63°$ can be extracted for the Al angular yield curve. The corresponding value calculated from Eq. (1) is $\Psi_{1/2} = 0.64°$, considering the channeling of the 2-MeV He^+ ions along the $\langle 0001 \rangle$-Al_2O_3 axis, and corundum crystal structure for Al_2O_3 with appropriate cell parameters [9] and r.m.s. thermal displacements [34]. In this case the energy loss of He projectiles in the Ga_2O_3 layer, as well as small-angle multiple scattering induced slight deflections [41] and direct backscattering of the analysing ions in the Ga_2O_3 layer (especially at around the interface) have been neglected in the calculation. In fact, we estimate a weak influence of such factors on the critical angle. The relatively high value of χ_{min} for Al is due to the reduced fraction of channeled ions in the analyzing beam passing through the Ga_2O_3 layer and the interface before encountering sapphire. Even though χ_{min} for Al is relatively high (~0.2), it is still lower than χ_{min} for Ga in the interface region (~0.3 at about channel no. 455, see Fig. 1(a)), thus revealing a significantly lower amount of defects and strain as sources of ion beam deflection and dechanneling on the substrate side. Nevertheless, there is a substantial agreement between calculated and measured $\Psi_{1/2}$ values for Al, thus demonstrating the applicability of the continuum steering potential model for the α-Al_2O_3 substrate. From a previous work [42], critical angles of $\Psi_{1/2} \approx 0.75°$, and $\Psi_{1/2} \approx 0.42°$ can be estimated for Al and O from 1.6 MeV He^+ axial channeling performed on $\langle 0001 \rangle$ oriented α-Al_2O_3. In good agreement, Eq. (1) gives $\Psi_{1/2} \approx 0.72°$, and $\Psi_{1/2} \approx 0.418°$, for Al and O, respectively.

3.2. RBS/C measurements on annealed Ga_2O_3

Fig. 4 shows the random RBS and best oriented RBS/C spectra of a thin layer Ga_2O_3 sample after annealing at 1000 °C for 2 h with a slow cooling rate (2 °C/min) [5]. In this case we were unable to find an axial channeling direction with satisfactorily low minimum yield for Ga. Compared to the random spectrum, only a relatively small drop in the Ga
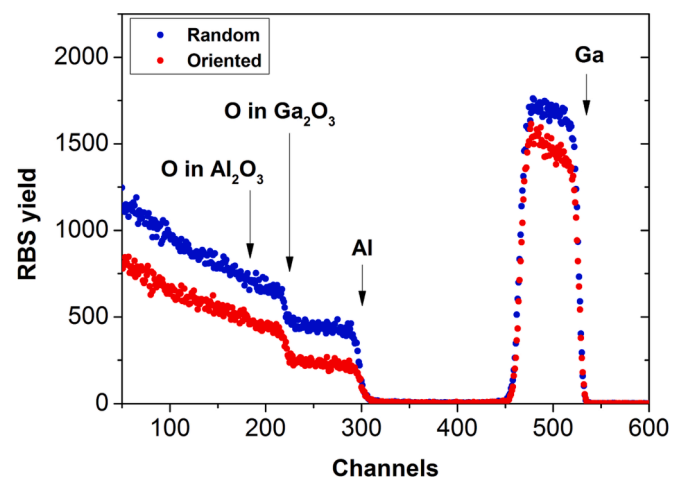

Fig. 4. Random and oriented 2-MeV He^+ RBS/C spectra of a Ga_2O_3 layer epitaxially grown on Al_2O_3 substrate and annealed at 1000 °C for 2 h and cooled down at 2 °C/min. Spectrum edges for different elements in the thin layer and in the underlying substrate are indicated.

RBS yield can be observed for the oriented case. A most significant drop in the channeling backscattering yield can be observed for the Al spectrum as compared to the random Al signal. This fact reveals better channeling conditions for the sapphire substrate than for the annealed Ga_2O_3 layer. After annealing at 1000 °C for 2 h followed by relatively slow cooling, the converted β-Ga_2O_3 layer assumed the standard (−201) orientation parallel to the c-axis of the Al_2O_3 substrate. TEM and XRD revealed a polycrystalline but defected/strained structure of this β-Ga_2O_3 layer [5]. These findings may explain the different channeling behaviour of the samples before and after heat treatment, i.e., crystalline phase transition. As expected from Table 1, ⟨-201⟩ oriented β-Ga_2O_3 may show inherently narrower angular widths for channeling as compared to ⟨0001⟩ oriented ε-Ga_2O_3. In addition, slight misalignment of the small crystallites, as well as the presence of defects or strain may induce blocking of the channels and distortion of the crystalline planes thus reducing the probability of channeling in the annealed thin layer. However, some channeling can still be observed due to the basically crystalline nature of the film.

Quite similar RBS/C behaviour was observed for another Ga_2O_3 sample (not shown here) which has been annealed at 1000 °C for 6 h with higher cooling rate (7.5 °C/min) [5]. The difference in the channeling characteristics compared to the unannealed sample reveals significant structural changes in the epitaxial layer during the annealing process. Indeed, previous TEM experiments performed on the same sample [5] showed, in particular, that after annealing at 1000 °C for 6 h followed by rapid cooling the film was entirely composed of β-Ga_2O_3 grains, most of them with (310) orientation with respect to the sapphire substrate.

The β-phase is known to accommodate ⟨-201⟩ orientation on sapphire (see [6] and refs. therein), and, being the thermodynamically most stable polymorph, it is worth considering its characteristic behaviour in ion beam channeling experiments. From the channeling point of view, single-crystalline β-Ga_2O_3 may be approximated with a face centered cubic (FCC) lattice of oxygen atoms [4], containing Ga atoms with octahedral/tetrahedral (O_h/T_d) site occupancy of 1:1 [10,43], see the schematics in Fig. 3(b). T_d sites occupy midpoints of the FCC cube edges and the cube center, while O_h sites are located in the centres of the eight half-sized cubes inherited by the FCC cubic cell. Considering that the atoms located on cube surfaces and in cube apices are shared by adjacent cells, the FCC cell contains four oxygen atoms, four O_h sites and eight T_d sites. The Ga atoms occupy only a fraction of the interstitial sites according to the Ga:O stoichiometry. Here we consider random occupancy of the suitable interstitial sites by Ga atoms.

For the FCC structure in Fig. 3(b) a cell parameter value of a ≈ 4.1 Å can be considered. In general, the β-phase is described by a monoclinic structure with cell parameters a = 12.21 Å, b = 3.03 Å, and c = 5.75 Å [44]. Fig. 3(b) is based on a simplified model of the oxygen lattice of β-Ga_2O_3 [4] which allows the estimation of the atomic composition and atomic spacing in ⟨-201⟩ oriented atomic rows from the sense of channeling.

For the crystal structure in Fig. 3(b), several different atomic rows can be viewed along the ⟨-201⟩ direction, with relatively large interatomic spacings. Each individual atomic row is monoatomic, i.e., contains only Ga or only O atoms, and, in general, the critical angle for channeling is quite low for all of them (see Table 1). Up to our knowledge a detailed axial channeling angular yield scan for β-Ga_2O_3 has not been reported so far, however ion beam channeling spectra have been shown for implanted and virgin β-Ga_2O_3 crystals. Typical minimum yields for Ga in virgin crystals varied in the range from few percents up to ∼ 10% [11–13], probably depending on crystal quality and ion beam parameters used in the channeling experiments. The detailed description of the β-Ga_2O_3 polymorph by RBS/C experiments seems to require further investigation. Usually, effective channeling cannot be achieved on polycrystalline materials if the size of the crystal grains is significantly smaller than the size of the ion beam applied in RBS/C experiments (typically on the 0.1–1 mm range). Better RBS channeling

conditions are expected for as-deposited single-crystalline β-Ga_2O_3 layers (compared to the polycrystalline β-phase material obtained via annealing) that we will grow in the near future. Proper channeling conditions achieved in RBS/C analysis are expected to allow direct comparison between experimental and calculated critical angles for channeling and minimum yields for the Ga and O sublattice of the β-Ga_2O_3 polymorph.

3.3. Spectroscopic ellipsometry measurements

The Ψ and Δ spectra measured by ellipsometry at multiple angles of incidence were fitted using an optical model that consists of an Al_2O_3 substrate and the Ga_2O_3 layer. A reference dielectric function from the Woollam database was used for the substrate, whereas the dispersion of the optical properties of the layer was described by polynomials, utilizing the B-spline method [45]. This approach gains increasing attention [46,47], because the application of oscillator models raises problems in materials with complicated band structure [48,49], in which the application of a bunch of generalized oscillators have no first principles-related physical meaning anymore. However, if the range of photon energies is limited to the sub-bandgap region, simple dispersion models can be used with a few fit parameters [49]. This approach was used in the present investigations to make sure that the proper thickness was applied in the B-spline model. The vertical inhomogeneity inferred from the RBS spectra and from previous TEM analysis was also modeled applying a double-layer structure for the Ga_2O_3 film using a Cauchy dispersion in both sublayers, but a better fit was obtained by a vertically graded single-layer B-spline model (Fig. 5). Assuming a nanoscale surface roughness neither improved the fit nor influenced the values of the fitted parameters, therefore, it was neglected.

As we will show in this section, while similarly weak RBS channeling effect was observed for both annealed ε-Ga_2O_3 layers, significant differences were found for these two samples by spectroscopic ellipsometry measurements.

The dielectric functions determined by SE show remarkable differences especially in the photon energy range near the band gap (E_g), see Fig. 6. The absorption edges shown by the ϵ_2 spectra between 4.5 and 5.5 eV are shifted to lower photon energies revealing a decrease of E_g with increasing annealing time. These features can be related to the observed phase transition [5] and to the different preferential orientations, ⟨-201⟩ and ⟨310⟩ of the converted β-Ga_2O_3 layer with respect to the substrate, as well as the presence of residual defects and strain after annealing. The increase of ϵ_2 in the full energy range can be observed for the 2 h annealed sample. For 6 h annealing, beside the further increase
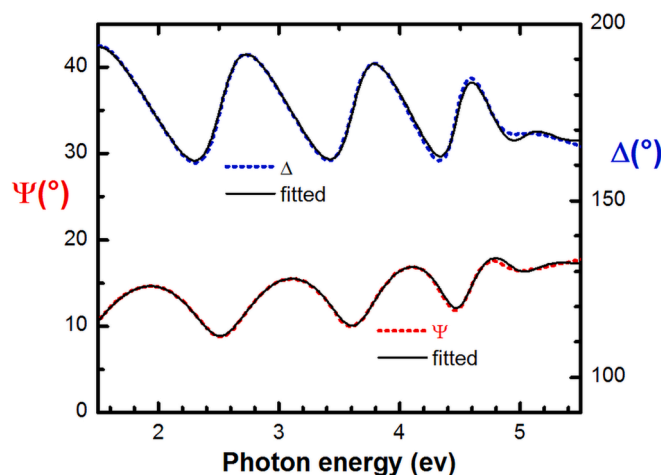

Fig. 5. Example of measured (colored dotted lines) and fitted (black solid lines) ellipsometry spectra on the as-deposited Ga_2O_3 layer the thickness of which is 279 nm. The angle of incidence corresponding to the plotted spectra was 55°.
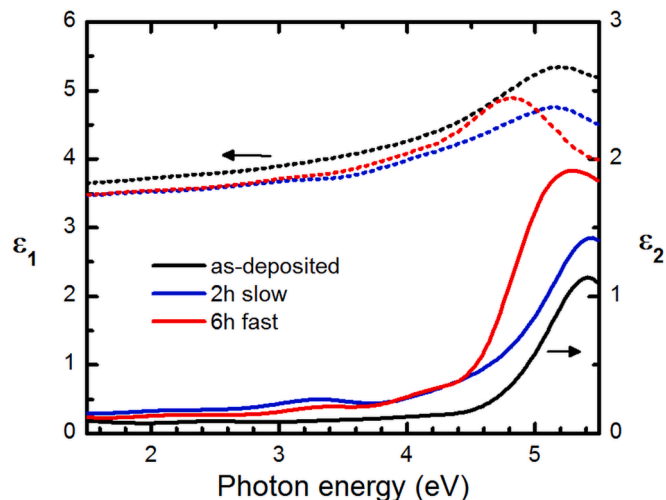
Fig. 6. Real (ϵ_1) and imaginary (ϵ_2) parts of the dielectric functions for as-grown and post annealed Ga_2O_3 layers measured by SE. The terms „2h slow" and „6h fast" apply to the annealing times and cooling phases.

of ϵ_2 above 4.5 eV photon energy, a remarkable shift can be observed for the absorption edge position in Fig. 6. This feature is probably related to the above mentioned orientational and structural differences between the films exposed to different annealing/cooling treatment conditions. It is expected that longer annealing and quick cooling will result in higher defect density, in addition to a frozen (3 1 0) prevalent orientation of grains in the converted β-Ga_2O_3 film.

Concerning hexagonal or pseudo-hexagonal phases, a bandgap of E_g = 4.9 eV was reported for ϵ-Ga_2O_3 grown by halid vapor phase epitaxy (HVPE) [50] and for ϵ-Ga_2O_3 grown by MIST-CVD technique on α-Al_2O_3 substrate [51]. In another work [52] E_g = 5.06 eV was found for κ-Ga_2O_3 on c-plane Al_2O_3, while B3LYP-DFT calculations resulted in a direct (indirect) bandgap of 5.08 eV (5.03 eV) for the hexagonal α-Ga_2O_3 polymorph [53].

For the monoclinic phase β-Ga_2O_3, experimental bandgap values of E_g = 4.72–4.74 eV [19] and E_g = 4.7 eV [54] were reported, while B3LYP-DFT calculations [53] resulted in a direct (indirect) bandgap of 4.69 eV (4.66 eV).

Extrapolation of the linear fits to our $(\alpha h\nu)^2$ versus $h\nu$ plots (not shown here) resulted in bandgap values of ca. 4.95 eV, 4.9 eV, and 4.7 eV for the as-grown, 2 h annealed, and 6 h annealed Ga_2O_3 layers. Apparently, the E_g of the unannealed sample is close to that was reported for the ϵ-Ga_2O_3 and κ-Ga_2O_3 polymorphs, while the long term annealed sample exhibits similar E_g than it was previously reported for the β-phase. As we found, a shorter annealing time resulted in a moderate change of the evaluated bandgap with respect to that of the as-grown ϵ-Ga_2O_3 layer.

For ϵ_1 only slight differences can be observed between all the datasets shown in Fig. 6, especially at photon energies below 4 eV. The two annealed samples show very similar ϵ_1 values in the visible range, while for the as-grown layer somewhat higher dielectric constants can be observed. This difference may be partly associated with the distinct polymorphs with pseudo-hexagonal and monoclinic structure, as found before and after annealing, respectively. Our SE data trends agrees with experiments and calculations [19,53] performed for Ga_2O_3 in its hexagonal and monoclinic phase, showing a higher measured refractive index (with n = 1.92–1.95) for the former as compared to the latter (with n = 1.84–1.89) structure. Calculation of the refractive indices in the zero-temperature, zero-frequency limit resulted in n = 1.74 and n = 1.68 [53] while bandgap corrected calculations give n = 1.95 and n = 1.87 [44] for hexagonal and monoclinic Ga_2O_3, respectively. In our case the refractive indices found for unannealed (ϵ-phase) and 2 h and 6 h annealed (β-phase) samples are n = 1.96, 1.90, and 1.91, respectively, at

a photon energy of 1.5 eV (see Fig. 6). This observed trend is consistent with the calculations perfomred for the different polymorphs. Also, our values for the annealed samples agree well with that found in Ref [19] for β-Ga_2O_3 at similar photon energy.

It is relevant to note that the dielectric spectra measured in the annealed Ga_2O_3 films of this study are not as sharp as the single-crystalline ones of Ref. [20]. This is to be expected as the monoclinic material studied here is the result of thermally-induced phase-transition, which – as already mentioned above - provides a β-polycrystalline layer with no long-range orientation, which is not directly comparable to as-deposited β-Ga_2O_3 thin films [19,21]. Furthermore, since the spot size used by SE is much larger than the dimension of nanometer grains, no optical anisotropy can be detected in the Ga_2O_3 layer. The obtained optical spectra represent an average response from the different in-plane orientations of the domains.

4. Conclusions

In this work the crystallographic structure of ϵ-Ga_2O_3 layers grown by MOVPE on Al_2O_3 substrate has been analyzed. The width and minimum yield of angular scan curves recorded by Rutherford Backscattering Spectrometry/Channeling (RBS/C) on the Ga and O sublattices were compared to calculations based on the continuum steering potential model. Good agreement between experiments and calculations was found when considering that the crystal structure of as-grown ϵ-Ga_2O_3 consists of oxygen atoms arranged in a 4H hexagonal closely packed (HCP) lattice in which Ga atoms preferentially occupy octahedral interstitial sites. These results are fully compatible with the ϵ-phase of Ga_2O_3 as it was previously shown by XRD and TEM measurements. High temperature annealing leads to transformation from the ϵ-phase to the monoclinic β-phase in the Ga_2O_3 film. This annealing-related structural reorganization led to remarkable changes in the RBS/C spectra. Our predictions show large differences in the width of the angular yield scan curves for $\langle 0001 \rangle$ axial channeling in the 4H lattice of the ϵ-phase and for $\langle -201 \rangle$ axial channeling in the FCC lattice of the β-phase, thus assigning the Ga and O angular yields as indicators for different Ga_2O_3 polymorphs.

In addition to RBS/C, spectroscopic ellipsometry (SE) measurements were carried out. SE was found to be an effective technique to distinguish between as-grown, initially ϵ-phase Ga_2O_3, and its annealed states containing essentially β-phase Ga_2O_3 crystallites. Significant differences in the evaluated dielectric functions were found before and after heat treatment, especially in the wavelength region around the bandgap. The observed trends may be related to phase transition from hexagonal to monoclinic structure, variation of the preferred crystallographic orientation of the β-phase with respect to the Al_2O_3 substrate after annealing, as well as to differences in residual strain and defect structure determined by the annealing conditions, such as duration and cooling rate.

Our results provide a valuable contribution to the identification of the structure of Ga_2O_3 crystals through monitoring of basic material properties. The application and further development of the RBS/C technique combined with SE is straightforward for high resolution in-depth analysis of as-grown and annealed epitaxial Ga_2O_3 layers. In future experiments, layer density changes induced by phase transitions at high temperature, high concentration doping, implantation-induced disorder formation, or annealing-induced recrystallization of the Ga_2O_3 matrix, can be followed by RBS/C combined with SE. In addition, RBS/C can provide information about the localization and activation of dopant atoms, like Sn or Si, in crystalline Ga_2O_3. Using our concept, ion implantation-induced disorder formation and annealing induced defect recovery processes as a function of depth, as well as changes in the atomic structure and optical properties of different Ga_2O_3 polymorphs can be followed for the fundamental technological steps.

CRediT authorship contribution statement

Z. Zolnai: Conceptualization, Methodology, Writing – review & editing. **P. Petrik:** Methodology, Writing – review & editing. **A. Németh:** Methodology. **J. Volk:** Writing – review & editing. **M. Bosi:** Methodology, Writing – review & editing. **L. Seravalli:** Methodology. **R. Fornari:** Conceptualization, Methodology, Writing – review & editing.

Declaration of Competing Interest

The authors declare that they have no known competing financial interests or personal relationships that could have appeared to influence the work reported in this paper.

Data availability

Data will be made available on request.

Acknowledgements

References

[1] Gallium Oxide: Technology, Devices and Application, ed. S. Pearton, F. Ren, and M. Mastro, Elsevier, 2018, ISBN: 9780128145210 (e-book), ISBN: 9780128145227 (Imprint).

[2] R. Roy, V.G. Hill, E.F. Osborn, Polymorphism of Ga_2O_3 and the system Ga_2O_3-H_2O, J. Am. Chem. Soc. 74 (1952) 719.

[3] L. Li, W. Wei, M. Behrens, Synthesis and characterization of α-, β-, and γ-Ga_2O_3 prepared from aqueous solutions by controlled precipitation, Solid State Sci. 14 (2012) 971.

[4] H.Y. Playford, A.C. Hannon, E.R. Barney, R.I. Walton, Structures of uncharacterised polymorphs of gallium oxide from total neutron diffraction, Chem. - A Eur. J. 19 (2013) 2803.

[5] R. Fornari, M. Pavesi, V. Montedoro, D. Klimm, F. Mezzadri, I. Cora, B. Pécz, F. Boschi, A. Parisini, A. Baraldi, C. Ferrari, E. Gombia, M. Bosi, Thermal stability of ε-Ga_2O_3 polymorph, Act. Mater. 140 (2017) 411.

[6] M. Bosi, P. Mazzolini, L. Seravalli, R. Fornari, Ga_2O_3 polymorphs: tailoring the epitaxial growth conditions, J. Mater. Chem. C 8 (2020) 10975.

[7] M. Bosi, L. Seravalli, P. Mazzolini, F. Mezzadri, R. Fornari, Thermodynamic and kinetic effects on the nucleation and growth of ε/κ- or β-Ga_2O_3 by metal–organic vapor phase epitaxy, Cryst. Growth Des. 21 (2021) 6393, https://doi.org/10.1021/acs.cgd.1c00863.

[8] S.-C. Zhu, S.-H. Guan, Z.-P. Liu, Mechanism and microstructures in Ga_2O_3 pseudomartensitic solid phase transition, Phys. Chem. Chem. Phys. 18 (2016) 18563.

[9] F. Mezzadri, G. Calestani, F. Boschi, D. Delmonte, M. Bosi, R. Fornari, Crystal structure and ferroelectric properties of ε-Ga_2O_3 films grown on (0001)-sapphire, Inorg. Chem. 55 (2016) 12079.

[10] I. Cora, F. Mezzadri, F. Boschi, M. Bosi, M. Caplovicova, G. Calestani, I. Dódony, B. Pécz, R. Fornari, The real structure of ε-Ga_2O_3 and its relation to κ-phase, CrystEngComm. 19 (2017) 1509.

[11] K. Lorenz, M. Peres, M. Felizardo, J.G. Correia, L.C. Alves, E. Alves, I. López, E. Nogales, B. Méndez, J. Piqueras, M.B. Barbosa, J.P. Araújo, J.N. Gonçalves, J. Rodrigues, L. Rino, T. Monteiro, E.G. Víllora, K. Shimamura, Doping of Ga_2O_3 bulk crystals and NWs by ion implantation, Proc. SPIE 8987 (2014) 89870M–M89871.

[12] E. Wendler, E. Treiber, J. Baldauf, S. Wolf, C. Ronning, High-level damage saturation below amorphisation in ion implanted β-Ga_2O_3, Nucl. Instrum. Methods Phys. Res. B 379 (2016) 85.

[13] E. Wendler, E. Treiber, J. Baldauf, S. Wolf, A. Kuramata, C. Ronning, Radiation effects in ion implanted β-Ga_2O_3, Proc. 11th Int. Conf. Interaction of Radiation with Solids, Sept. 23-25, 2015, Minsk, Belarus, (2015) p. 93.

[14] S. Yadav, S. Dash, A.K. Patra, G.R. Umapathy, S. Ojha, S.P. Patel, R. Singh, Y. S. Katharria, Effects of energetic ion irradiation on β-Ga_2O_3 thin films, ECS J. Solid State Sci. Tech. 9 (2020), 045015.

[15] Z. Zolnai, A. Ster, N.Q. Khánh, G. Battistig, T. Lohner, J. Gyulai, E. Kótai, M. Posselt, Damage accumulation in nitrogen implanted 6H-SiC: dependence on the direction of ion incidence and on the ion fluence, J. Appl. Phys. 101 (2007), 023502.

[16] W. Jiang, W.J. Weber, Multiaxial channeling study of disorder accumulation and recovery in gold-irradiated 6H-SiC, Phys. Rev. B 64 (2001), 125206.

[17] A. Azarov, V. Venkatachalapathy, P. Karaseov, A. Titov, K. Karabeshkin, A. Struchkov, A. Kuznetsov, Interplay of the disorder and strain in gallium oxide, Sci. Rep. 12 (2022) 15366.

[18] A. Bosio, A. Parisini, A. Lamperti, C. Borelli, L. Fornasini, M. Bosi, I. Cora, Z. Fogarassy, B. Pécz, Z. Zolnai, A. Németh, S. Vantaggio, R. Fornari, n-type doping of ε-Ga_2O_3 epilayers by high-temperature tin diffusion, Act. Mater. 210 (2021), 116848.

[19] M. Rebien, W. Henrion, M. Hong, J.P. Mannaerts, M. Fleischer, Optical properties of gallium oxide thin films, Appl. Phys. Lett. 81 (2002) 250, https://doi.org/10.1063/1.1491613.

[20] C. Sturm, J. Furthmüller, F. Bechstedt, R. Schmidt-Grund, M. Grundmann, Dielectric tensor of monoclinic Ga_2O_3 single crystals in the spectral range 0.5–8.5 eV, APL Materials 3 (2015), 106106, https://doi.org/10.1063/1.4923345.

[21] M. Passlack, E.F. Schubert, W.S. Hobson, M. Hong, N. Moriya, S.N.G. Chu, K. Konstadinidis, J.P. Mannaerts, M.L. Schnoes, G.J. Zydzik, Ga_2O_3 films for electronic and optoelectronic applications, J. Appl. Phys. 77 (1995) 686, https://doi.org/10.1063/1.359055.

[22] M. Zhao, R. Tong, X. Chen, T. Ma, J. Dai, J. Lian, J. Ye, Ellipsometric determination of anisotropic optical constants of single phase Ga_2O_3 thin films in its orthorhombic and monoclinic phases, Opt. Mater. 102 (2020), 109807.

[23] T. Onuma, S. Saito, K. Sasaki, T. Masui, T. Yamaguchi, T. Honda, A. Kuramata, M. Higashiwaki, Spectroscopic ellipsometry studies on β-Ga_2O_3 films and single crystal, Jpn. J. Appl. Phys. 55 (2016) 1202B2.

[24] B.R. Tak, S. Kumar, A.K. Kapoor, D. Wang, X. Li, H. Sun, R. Singh, Recent advances in the growth of gallium oxide thin films employing various growth techniques – a review, J. Phys. D 54 (2021), 453002.

[25] N.Q. Khánh, Z. Zolnai, T. Lohner, L. Tóth, L. Dobos, J. Gyulai, He ion beam density effect on damage induced in SiC during Rutherford backscattering measurement, Nucl. Instrum. Methods Phys. Res. B 161–163 (2000) 424.

[26] F. Pászti, A. Manuaba, C. Hajdu, A.A. Melo, M.F. Da Silva, Current measurement on MeV energy ion beams, Nucl. Instrum. Methods Phys. Res. B 47 (1990) 187.

[27] E. Szilágyi, E. Kótai, D.G. Merkel, Ion-beam analysis of insulator samples, Nucl. Instrum. Methods Phys. Res. B 450 (2019) 184–188.

[28] E. Kótai, Computer methods for analysis and simulation of RBS and ERDA spectra, Nucl. Instrum. Methods Phys. Res. B 85 (1994) 588.

[29] D. Tamba, O. Kubo, M. Oda, S. Osaka, K. Takahashi, H. Tabata, K. Kaneko, S. Fujita, M. Katayama, Surface termination structure of α-Ga_2O_3 film grown by mist chemical vapor deposition, Appl. Phys. Lett. 108 (2016), 251602.

[30] Y. Xu, Z. J-h Park, C. Yao, M. Wolverton, J.W. Razeghi, V.P. Dravid, Strain-induced metastable phase stabilization in Ga_2O_3 thin films, ACS Appl. Mater. Interfaces 11 (5) (2019) 5536.

[31] K. Jiang, J. Tang, M.J. Cabral, A. Park, L. Gu, R.F. Davis, L.M. Porter, Layered phase composition and microstructure of κ-Ga_2O_3-dominant heteroepitaxial films grown via MOCVD, J. Appl. Phys. 131 (2022), 055305.

[32] J.H. Barrett, Monte Carlo channeling calculation, Phys. Rev. B 3 (1971) 1527.

[33] J.B. Marion, F.C. Young, Nuclear Reaction Analysis, North-Holland Publishing Co., Amsterdam, 1968.

[34] E.A. Soares, M.A. Van Hove, C.F. Walters, K.F. McCarty, Structure of the α-Al_2O_3 (0001) surface from low-energy electron diffraction: Al termination and evidence for anomalously large thermal vibrations, Phys. Rev. B 65 (2002), 195405.

[35] E. Alves, M.F. da Silva, G.N. van den Hoven, A. Polman, A.A. Melo, J.C. Soares, Incorporation and stability of erbium in sapphire by ion implantation, Nucl. Instrum. Methods Phys. Res. B 106 (1995) 429.

[36] A. Redondo-Cubero, M. Vinnichenko, M. Krause, A. Mucklich, E. Munoz, A. Kolitsch, R. Gago, Sublattice-specific ordering of ZnO layers during the heteroepitaxial growth at different temperatures, J. Appl. Phys. 110 (2011), 113516.

[37] J. Albertsson, S.C. Abrahams, Atomic displacement, anharmonic thermal vibration, expansivity and pyroelectric coefficient thermal dependences in ZnO, Acta Cryst. B45 (1989) 34.

[38] S. Stelmakh, E. Grzanka, M. Wojdyr, T.h. Proffen, S.C. Vogel, T.W. Zerda, W. Palosz, B. Palosz, Neutron diffraction studies of the atomic thermal vibrations in complex materials: application of the Wilson method to examination of micro- and nano-crystalline SiC, Zeitschrift für Kristallographie 222 (2007) 174.

[39] J.M. Lombaard, O. Meyer, Channeling studies in carbon implanted NbC-single crystals, Rad. Eff. 36 (1978) 83.

[40] I. Nashiyama, T. Nishijima, E. Sakuma, S. Yoshida, Deuteron channeling for defects analysis of silicon carbide, Nucl. Instrum. Methods Phys. Res. B 33 (1988) 599.

[41] M. Mayer, P. Malinský, F. Schiettekatte, Z. Zolnai, Intercomparison of ion beam analysis software for the simulation of backscattering spectra from two-dimensional structures, Nucl. Instrum. Methods Phys. Res. B 385 (2016) 65.

[42] G.N. van den Hoven, A. Polman, E. Alves, M.F. da Silva, A.A. Melo, J.C. Soares, Lattice site and photoluminescence of erbium implanted in α-Al$_2$O$_3$, J. Mater. Res. 12 (1997) 1401.

[43] J. Åhman, G. Svensson, J. Albertsson, A reinvestigation of β-Gallium Oxide, Acta Crystallogr. C: Cryst. Struct. Commun. 52 (1996) 1336.

[44] F. Litimein, D. Rached, R. Khenata, H. Baltache, FPLAPW study of the structural, electronic, and optical properties of Ga$_2$O$_3$: monoclinic and hexagonal phases, J. Alloys Compd. 488 (2009) 148.

[45] B. Johs, J.S. Hale, Dielectric function representation by B-splines, Phys. Stat. Sol. (a) 205 (2008) 715, https://doi.org/10.1002/pssa.200777754.

[46] D.V. Likhachev, On the optimization of knot allocation for B-spline parameterization of the dielectric function in spectroscopic ellipsometry data analysis, J. Appl. Phys. 129 (2021), 034903, https://doi.org/10.1063/5.0035456.

[47] D.V. Likhachev, Certain topics in ellipsometric data modeling with splines: a review of recent developments, Adv. Opt. Technol. 11 (2022) 93, https://doi.org/10.1515/aot-2022-0006.

[48] P. Petrik, Parameterization of the dielectric function of semiconductor nanocrystals, Physica B: Cond. Mat. 453 (2014) 2, https://doi.org/10.1016/j.physb.2014.03.065.

[49] E. Agócs, B. Fodor, B. Pollakowski, B. Beckhoff, A. Nutsch, M. Jank, P. Petrik, Approaches to calculate the dielectric function of ZnO around the band gap, Thin Solid Films. 571 (2014) 684, https://doi.org/10.1016/j.tsf.2014.03.028.

[50] Y. Oshima, E.G. Víllora, Y. Matsushita, S. Yamamoto, K. Shimamura, Epitaxial growth of phase-pure ε-Ga$_2$O$_3$ by halide vapor phase epitaxy, J. Appl. Phys. 118 (2015), 085301.

[51] S. Yusa, D. Oka, T. Fukumura, High-κ dielectric ε-Ga$_2$O$_3$ stabilized in a transparent heteroepitaxial structure grown by mist CVD at atmospheric pressure, CrystEngComm. 22 (2020) 381.

[52] A F M Anhar Uddin Bhuiyan, Z. Feng, H.-L. Huang, L. Meng, J. Hwang, and H. Zhao, MOCVD growth and band offsets of κ-phase Ga$_2$O$_3$ on c-plane sapphire, GaN- and AlN-on-sapphire, and (100) YSZ substrates, J. Vac. Sci. Technol. A 40 (2022) 062704.

[53] H. He, R. Orlando, M.A. Blanco, R. Pandey, E. Amzallag, I. Baraille, M. Rérat, First-principles study of the structural, electronic, and optical properties of Ga$_2$O$_3$ in its monoclinic and hexagonal phases, Phys. Rev. B 74 (2006), 195123, and refs. therein.

[54] H.H. Tippins, Optical absorption and photoconductivity in the band edge of β-Ga$_2$O$_3$, Phys. Rev. 140 (1965) A316.